Account

Excitation Energy Migration in Multiporphyrin Arrays

In-Wook Hwang, Naoki Aratani,[†] Atsuhiro Osuka,[†,*] and Dongho Kim[*]

*National Creative Research Initiatives Center for Ultrafast Optical Characteristics Control and
Department of Chemistry, Yonsei University, Seoul 120-749, Korea. [*]E-mail: dongho@yonsei.ac.kr
[†]Department of Chemistry and Core Research for Evolutional Science and Technology (CREST),
Kyoto University, Kyoto 606-8502, Japan. [*]E-mail: osuka@kuchem.kyoto-u.ac.jp*

During the last decade, the exploration of nanoscale device and circuitry based on molecules has gained increasing interest. In parallel with this, considerable effort is being devoted to the development of molecular photonic/electronic materials based on various porphyrin arrays. This involves light as an input/output signal and excitation energy migration as a mechanism for signal transmission. Absorption of a photon at the light collector end of the porphyrin array yields the excited state, which migrates among the intervening pigments until reaching the emitter, whereupon another photon is emitted. As a consequence, it is relevant to understand the excitation energy transfer (EET) processes occurring in various forms of porphyrin arrays for the applications as artificial light harvesting arrays and molecular photonic/electronic wires. Since the excitonic (dipole) and electronic (conjugation) couplings between the adjacent porphyrin moieties in porphyrin arrays govern the EET processes, we have characterized the EET rates of various forms of multiporphyrin arrays (linear, cyclic, and box) based on various time-resolved spectroscopic measurements. We believe that our observations provide a platform for further development of molecular photonic/electronic materials based on porphyrin arrays.

Key Words : Energy transport, Porphyrin arrays, Time-resolved spectroscopy, Dipole coupling, Light harvesting arrays

Introduction

The primary process in photosynthesis is initiated by absorption of light in the light-harvesting antenna and subsequent excitation energy transfer (EET) to the reaction center. Besides the numerous researches on the natural light harvesting complexes,[1,2] the mimicry of them has been continuously attempted by designing various artificial multi-porphyrin systems with an aim of achieving highly efficient and directional EET processes.[3] Until now, we have designed various strongly coupled porphyrin arrays (linear,

cyclic, and box) and investigated their EETs with ultrafast time-resolved laser spectroscopy.[4,5] A fine control of EET process, however, would be realized by adjusting the excitonic coupling between the adjacent porphyrin units. By exploring the exciton coupling dynamics, we can gain further insight into the relationship of EET rate with the configuration of the porphyrin arrays.

From a viewpoint of operational requirement in molecular photonic/electronic devices, the porphyrin arrays should have regular pigment arrangement that allows a facile energy or charge flow but do not perturb the property of

In-Wook Hwang (b. 1972) grew up in Incheon, Korea. He received a B.S. in chemistry from Dankook University (1995) and a Ph.D. from Yonsei University (2002). After Ph.D. course, he joined the Center for Ultrafast Optical Characteristics Control in Yonsei University as a postdoctoral fellow (2002). Since 2005, he will join the Institute for Polymer and Organic Solids in University of California, Santa Barbara (the leader is Alan J. Heeger) through the Post-doctoral Fellowship Program by the Korea Science Engineering Foundation.

Naoki Aratani was born in 1975 in Nagoya, Japan. He received his B.Sc. degree in 1999 and his M.Sc. degree in 2001, both from Kyoto University. He was selected as a Research Fellow of the Japan Society for the Promotion of Science (JSPS) in 2001. During autumn 2002, as a visiting fellow, he worked with Professor Christopher A. Hunter's group in the Department of Chemistry at the University of Sheffield, UK. He is currently an assistant professor with Prof. A. Osuka at Kyoto University, focusing on the design and synthesis of extremely long porphyrin arrays for the exploration of the nature of giant molecules.

Atsuhiro Osuka (b.1954) grew up in Gamagori, Aich, Japan. He received a B.S. in chemistry (1977) and a Ph.D. from Kyoto University (1982). After 4 years as an Assistant Professor at Ehime University, he returned to Kyoto University, where he is Professor of Chemistry. Currently he is the leader of the Core Research for Evolutionary Science and Technology Project supported by the Japan Science and Technology Corporation.

Dongho Kim (b. 1957) grew up in Seoul, Korea. He received a B.S. in chemistry from Seoul National University (1980) and a Ph.D. from Washington University (1984). After postdoctoral research at Princeton University, he joined the Korea Research Institute of Standards and Science (1986). He moved to Yonsei University (2000), where he is Professor of Chemistry. Since 1997, he has been leading the Center for Ultrafast Optical Characteristics Control through the National Creative Research Initiatives Program supported by the Korea Science Engineering Foundation.
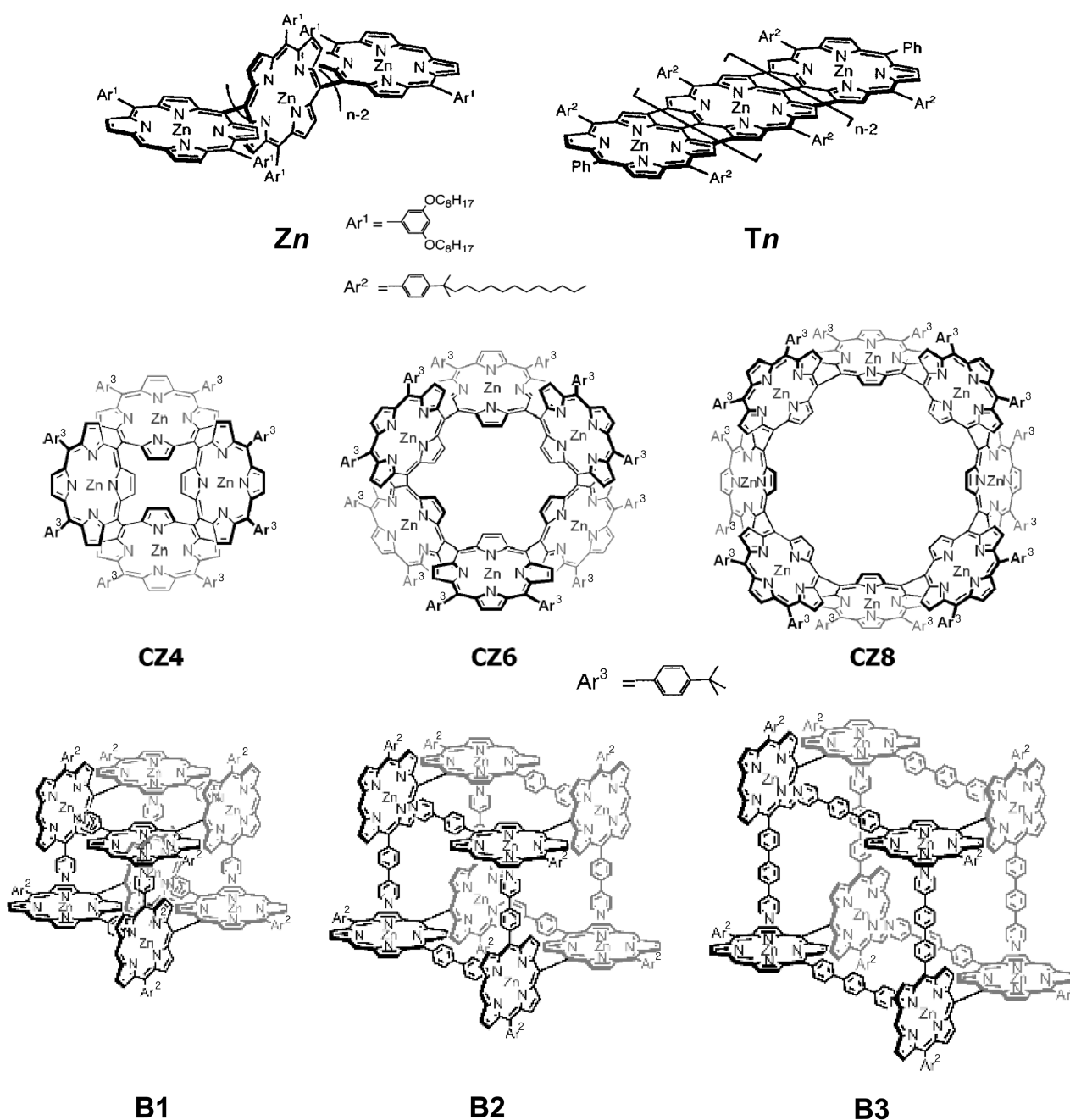
Zn $Ar^1 =$ (with OC_8H_{17}, OC_8H_{17})   **T*n***

$Ar^2 =$

CZ4   **CZ6**   **CZ8**

$Ar^3 =$

B1   **B2**   **B3**

Chart 1. Structures of **Z*n***, **T*n***, **CZ*n***, and **B*n***. Reproduced with permission from refs 8, 9, 14, and 18.

individual pigment. In this context, the directly-linked orthogonal and fused zinc(II) porphyrin arrays (**Z*n*** and **T*n***) are pertinent for the photonic and electronic devices, respectively, because the former has strong dipole coupling without electronic communication, while the latter is a well organized electron transmission system (Chart 1). Without the interporphyrin linker, the electronic perturbation by the linker and the conformational heterogeneity mainly arising from the dihedral angle distribution between porphyrin units are minimized in these directly linked porphyrin arrays. As a consequence, the orthogonal and fused porphyrin arrays would be one of the most suitable synthetic modules for the realization of molecular photonic and electronic wires.

Because the EET processes in natural light harvesting complexes (LH2 and LH1) are very efficient (>99%) and ultrafast (sub-picosecond),[2] the mimicry of the wheel-like giant architecture of photosynthetic pigments would also be highly desirable for the improved signal transmission in the optoelectronic devices.[6] To mimic the wheel-like architecture, two-dimensional cyclic porphyrin arrays (**CZ*n***) are constructed by direct and bidirectional inter-porphyrin connections at two *meso* positions of porphyrin monomer (Chart 1). Because the cyclic porphyrin arrays have well-defined architectures like LH1 and LH2, they can afford comprehensive EET mechanism, especially, the exciton coupling effect on the EET rate. According to the ultrafast spectro-

scopic measurement, the prepared cyclic porphyrin arrays interestingly show faster EET rates than LH1 and LH2, which makes them good candidates for artificial light harvesting devices.

As a supplementary route in the preparation of porphyrin arrays, a synthetic strategy utilizing supramolecular chemistry has been envisaged, because it provides versatility in molecular networking in multi-dimensional space.[7] In this regard, three-dimensional porphyrin boxes (**B***n*) are prepared by intermolecular coordination of four orthogonally-linked zinc(II) diporphyrin units (Chart 1). The distantly and directionally controlled porphyrin units along xyz-axes are ideal to elucidate the relationship between the EET rate and the coherent exciton coupling. In addition, the pigment orientation toward three-dimensional space is likely to increase the light-absorbing capability per unit cell, which is advantageous in optoelectronic application.

Overall, the regularly arranged porphyrin arrays with ample excitonic/electronic interactions are promising in the optoelectronic applications such as molecular photonic/ electronic wire, sensor, solar energy battery, optical nonlinear material, and so on. In this review, EET phenomena occurring in various porphyrin arrays (linear, cycle, and box) are comparatively described, in which the exciton coupling among constituent porphyrin pigments performs critical roles.

Linear Porphyrin Array

Exciton Coherence Coupling. Recently, we have prepared long *meso-meso* linked linear porphyrin arrays (**Z***n*, *n* = 2, 3…, Chart 1), in which the porphyrin units are orthogonally connected together up to 1024 units without any linkers.[8] According to our study, **Z***n* revealed fast EET rate *e.g.* (~200 fs)$^{-1}$ *via* strong exciton coupling between the adjacent porphyrin units, which can realize molecular photonic

Figure 1. Absorption spectra of (a) porphyrin monomer and **Z***n* from **Z2** to **Z128** and (b) **T***n* from **T2** to **T6** in CHCl$_3$. The background absorptions at ~6000, ~4000, and ~3500 cm^{-1}, in part b, result from the overtones of C-H vibration of the solvent. Reproduced with permission from refs 8c and 9a.

wire.[8b] On the other hand, the connection of porphyrin units with triple linkages, *i.e.*, *meso-meso*, *β-β*, and *β-β*, makes a completely flat architecture that has strong π-conjugation over the entire array, thus realizes molecular electronic wire (**T***n*, *n*=2, 3…12, Chart 1).[9]

Figure 1 shows the UV/visible/IR absorption spectra of **Z***n* and **T***n* that are normalized at 23,700 to 24,000 cm^{-1} and 23,800 to 24,600 cm^{-1} regions, respectively. The Soret bands of **Z***n* are largely split but the *Q*-bands remain nearly at the same positions with an increase of the array length. These spectral features have been ascribed mainly to the perpendicular conformation that can induce exciton coupling but cannot allow π-electron conjugation. Although two almost degenerate transition dipoles B_x and B_y create one Soret band in **Z1**, the excitonic dipole couplings between adjacent porphyrin units, such as B_z+B_z at opposite, B_x+B_y at orthogonal, and B_z+B_z at parallel, generate three non-degenerate transition dipoles and concomitantly two separate Soret bands of **Z2** (Scheme 1).[8b,c] On the contrary, the fully conjugated porphyrin tapes, **T***n*, display drastically red-shifted *Q*-bands that reach into far infrared region.[9] With an increase of porphyrin units, the $B_{x,y}$ bands remain nearly at the same positions as that of **Z1**, while the B_z and *Q* bands are continuously red-shifted along with an increase in their relative intensities (Figure 1b).

The systematic spectral change in the Soret bands of **Z***n* is explained in a qualitative manner by simple point-dipole exciton coupling model,[10] for which eq. 1 predicts the exciton splitting energy ΔE_0 between the neighboring porphyrin units,

$$\Delta E_0 = \frac{\mu^2}{2\pi\varepsilon_0 R^3} \quad (1)$$

where μ is the transition dipole moment of porphyrin unit and R is the center-to-center distance between the neighboring porphyrins (8.35 Å). The splitting energy ΔE of the longer arrays can also be given by eq. 2,

$$\Delta E = \Delta E_0 \cos[\pi/(N+1)] \quad (2)$$

where N is the number of porphyrin units and ΔE is doubling of the observed energy difference between the red-shifted B_z and unperturbed $B_{x,y}$ bands (Scheme 1).[8b,c] When ΔE values were plotted according to eq 2, a straight line with a slope of $\Delta E_0 = 4300$ cm^{-1} was obtained for the Soret bands of **Z***n*, indicating strong exciton coupling between the neighboring porphyrin units and well aligned porphyrin units as a linear form.[8b,c] However, the deviation from the linearity in the longer arrays (n > 16) proposed some conformational heterogeneity. In a similar manner, the exciton coupling strength in the S$_1$-state of **Z***n* was evaluated. The energy differences between the *Q*(1,0) bands of **Z1** and the porphyrin arrays (**Z2**-**Z16**) were plotted again according to eq. 2. As a result, we obtained a best fit line with a slope of 1140 cm^{-1} ($V = 570$ cm^{-1}), which was larger than $V = 280$ cm^{-1} that assumed only point dipole-dipole coupling between the porphyrin units. This, thus, indicates additional inter-
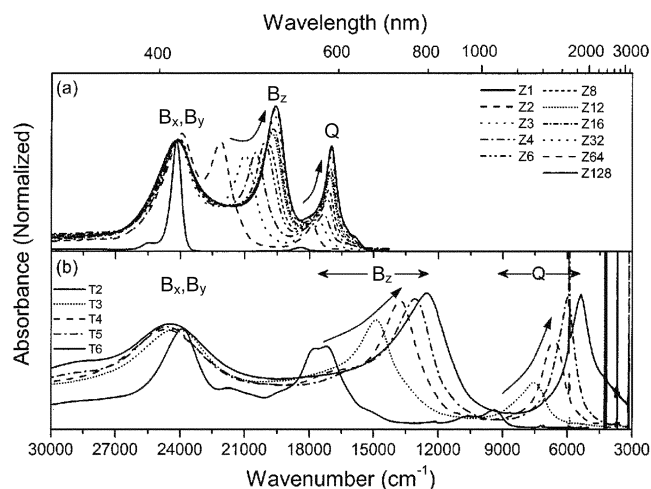
Scheme 1. Exciton couplings in zinc(II) porphyrin monomer (**Z1**), *meso-meso* linked zinc(II) diporphyrin (**Z2**), and three-dimensional zinc(II) porphyrin box (**B***n*). Reproduced with permission from refs 18b,c.

action besides point dipole-dipole coupling in the S_1-state of **Z***n*. The short distance between porphyrin units is believed not only to enhance through-space dipole-dipole coupling but also to increase through-bond interaction.[8c]

In contrast to **Z***n*, the extensive π-conjugation of **T***n* resulted in very different characteristics in terms of exciton coupling scheme. The observed linear plot for the energy difference between the $B_{x,y}$ and B_z bands as a function of the number of porphyrin units indicated that the absorption spectra were actually influenced by the exciton coupling scheme and the constituent porphyrin pigments were aligned linearly. The plot for the Q bands, however, was strongly deviated from the exciton coupling scheme. Instead, the plot based on free electron model (particle in a box model) resulted in a well-correlated straight line, indicating that the S_1-state of **T***n* could be characterized by the extensive π-conjugation throughout the array.[9b] The band shift as a function of the number of porphyrin units indicated that the B_z band exhibited a clear saturation behavior with the effective conjugation length (ECL) number of *ca.* 8, while the Q band did not show such saturation up to **T12**, *i.e.*, the ECL number of n > 12 in the S_1-state of **T***n*.[9]

Radiative Coherence Length. The exciton coherence length has been a central issue in the EET processes of molecular arrays, because the excitation energy hops among exciton coupled units that have intrinsic exciton coherence length. According to the empirical formula for one-dimensional linear array developed by Kakitani *et al.*,[11] the exciton coherence length N_c has been described by eq. 3,

$$N_C = 1.38 + 1.33\frac{V}{\gamma} \tag{3}$$

where V is the exciton coupling energy and γ is the homogeneous broadening in the absorption band. Using $V = 570$ cm^{-1} and $\gamma = 250$ cm^{-1} that were respectively obtained from **Z***n* and the spectral bandwidth in the Q-band of **Z1** at 103 K, we could observe the exciton coherence length of 4.5 porphyrin units in the **Z***n* array without inhomogeniety.[11c] With the inhomogeniety of 100-50 cm^{-1}, the coherence

Figure 2. Plot of the ratio between the radiative or nonradiative decay rates of **Z***n* and **Z1** as a function of the number of porphyrin units.

length was estimated as $N_c = \sim4$.

Another spectroscopic observable directly related to the exciton coherence length is superradiance (radiative coherence length).[8c] The radiative coherence length is defined as the ratio between the radiative decay rate of the array and that of the monomer, *i.e.*, $k_{array} = Nk_{monomer}$. To estimate the radiative coherence length, the ratios between the radiative decay rates of **Z***n* and **Z1** were plotted as a function of the number of porphyrin units (Figure 2). The deviation point (4-5 porphyrin units) from the linearity seemed to be a reasonable estimation of the radiative coherence length of **Z***n*, which is also in a good agreement with the calculated exciton coherent length. Consequently, the EET process occurs among the hopping sites consisting of 4.5 porphyrin units in the S_1-state of **Z***n*. It is noteworthy that the nonradiative decay rates of **Z***n* remain nearly the same with an increase of the number of porphyrin units in **Z***n* (Figure 2). This feature suggests that the nonradiative deactivation processes of **Z***n* are mainly contributed by the intramolecular in- and out-of-plane vibrational relaxation processes within the constituent porphyrin monomer unit. In other words, the deformation or tilting between the porphyrin units in **Z***n* does not play a significant role in enhancing the nonradiative decay rates in **Z***n*.

Conformational Heterogeneity. In view of practical use, it is important to know the morphology of the array. We, thus, analyzed the conformational heterogeneity of **Z***n* in terms of fluorescence spectra. The plot of the molar extinction coefficients of **Z***n* as a function of the number of porphyrin units exhibits a linear summation behavior up to **Z512**, indicating an independent light absorbing property of each porphyrin unit in the array. The fluorescence quantum yield, however, shows a maximum value at **Z16**, which reveals a gradual increase in going from **Z1** to **Z16** but decreases in the array longer than **Z16**, giving rise to a fast (~100 ps) fluorescence decay. In addition, the steady-state fluorescence excitation anisotropy monitored at 450-600 nm

e.g. low energy Soret and Q absorption bands shows the maximum value at **Z16** and starts to decrease as the array length further increases.[3] These features consistently indicate that the overall geometry of **Z***n* remains as linear form in the arrays shorter than **Z16** but start to deviate from the linearity in the array longer than **Z16**. As the array becomes bent, nonradiative quenching sites accelerate the fluorescence relaxation process and concomitantly reduce the fluorescence quantum yield. In addition, the fluorescence excitation anisotropy value decreases in the curved array, resulting from the nonlinearity in overall molecular dipole arrangements. Concerning the morphology, the STM measurement of **Z48** showed a crooked image although it gave even more curved structure intrinsically due to multiple interactions of **Z48** with the gold surface (Figure 3). Consequently, the conformational heterogeneity inevitably reduces the exciton coupling strength between the pigments in longer **Z***n* (n > 16), which is not advantageous in optoelectronic application. Further work, thus, will be focused on preparing the

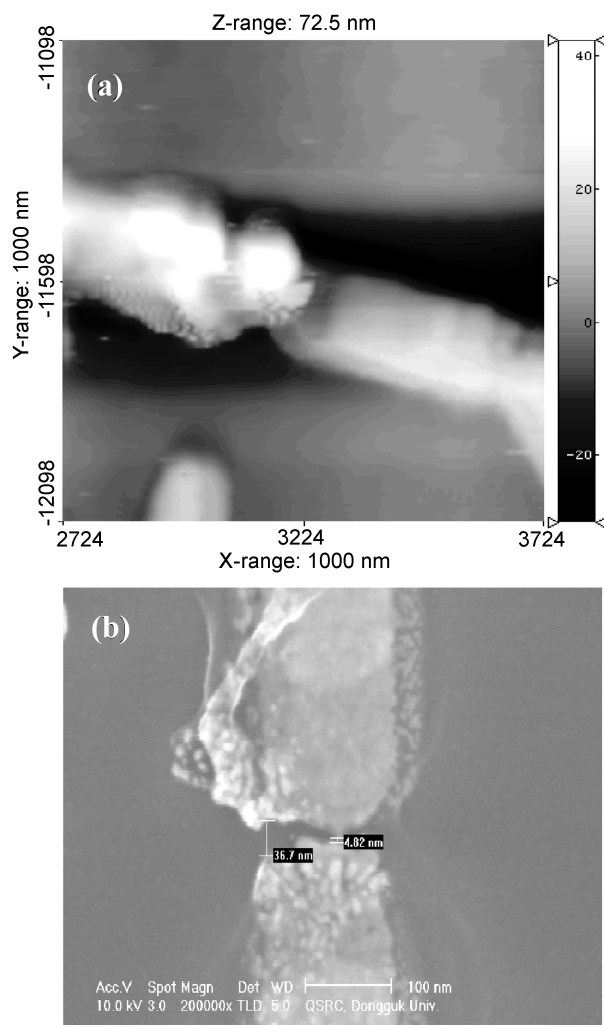**Figure 3**. Scanning tunneling microscope image of **Z48**. Reproduced with permission from ref 12.

Figure 4. (a) Atomic force microscope image of **Z48** trapped between two metal electrodes. (b) Field emission scanning electron microscope image of nanoelectrodes of **T8** fabricated by the electromigration induced break-junction technique. Reproduced with permission from ref 12.

longer and rigid **Z***n* array with good linearity, which can be realized by physical or chemical stretching and rigidification.

Electrical Conductance. To explore the electrical property, we have performed electrical transport measurements of two extreme types of porphyrin arrays (**Z48** and **T8**), where two kinds of Au/Ti nanoelectrodes were used for molecular level measurements.[12] For **Z48** with the length of about 40 nm, nanoelectrodes with a spacing of about 20-30 nm were fabricated by electron-beam lithography and a double-angle evaporation technique onto degenerately doped silicon substrate with a top SiO_2 layer of 0.5 μm (Figure 4a). On the other hand, for **T8** with about 7 nm in its length, Au/Ti nanoelectrodes with a spacing of less than 7 nm were prepared by utilizing the electromigration induced break-junction technique (Figure 4b). Electrical contact between porphyrin arrays and metal electrodes was made using the electrostatic trapping method. A drop of porphyrin solution (3 nmol) was positioned on the top of the electrode gap. Then, a voltage of up to 5 V was applied to the electrodes. After trapping the porphyrin array between electrodes, the sample was dried under nitrogen purging and characterized using a semiconductor characterization system (Keithley 4200). All electrical transport measurements were performed
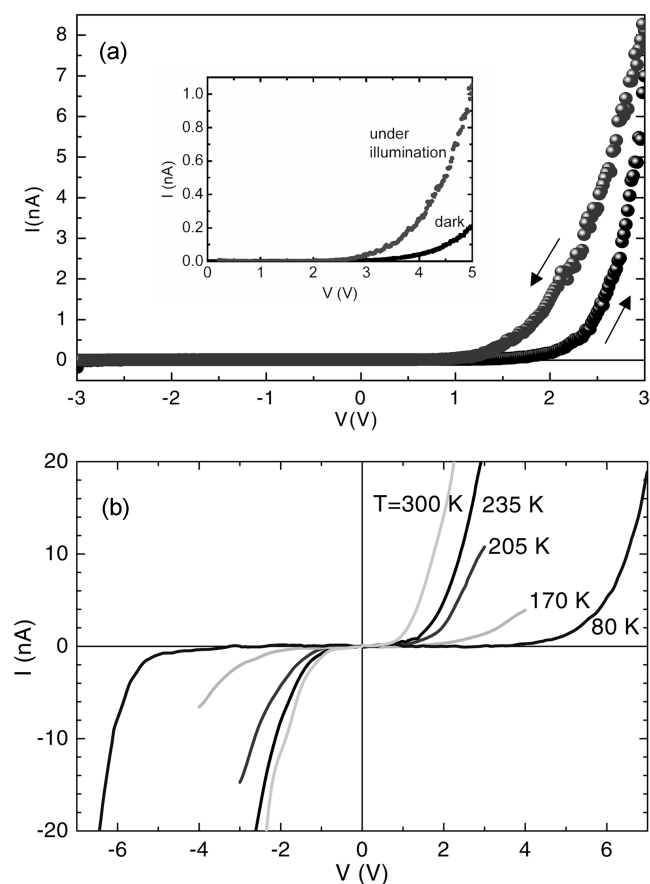
in vacuum to eliminate the effect of water on the conductance.

Figure 5a displays the *I-V* curve measured at room temperature for **Z48** trapped between two nanoelectrodes. It exhibits the hysteresis depending on the voltage sweep direction. From the slope of *I-V* curves, the room temperature resistance was estimated to be 125-670 MΩ, where the conductance was enhanced under illumination with a red LED, exhibiting a diode-like behavior of **Z***n* (Figure 5a, inset). In the temperature dependence on the *I-V* curve, the conductance was decreased very rapidly with lowering the temperature and no current was observed in the voltage range from −5 to +5 V at 180 K, indicating that the conductance was due to the conformational heterogeneity arising from the dihedral angle distribution between porphyrin units. Figure 5b shows the *I-V* curves measured at several temperatures for **T8**. In contrast to **Z48**, it is nearly symmetric without any hysteresis, implying that the rotation about *meso-meso* C-C bond does not occur in **T8**. Moreover, compared with **Z48** the higher conductance and the smaller voltage gap were found in **T8**. The room temperature resistance estimated from the slope of the *I-V* curve was about 50 MΩ that is smaller than 125-670 MΩ of **Z48**. This result indicates that the strong π-electron conjugation results in better electrical conduction in **T8**. In the temperature dependence on the *I-V* curve, the conductance of **T8** was slowly decreased and the voltage gap was widened with lowering the temperature, indicating that the conductance is not due to the dihedral angle distribution between porphyrin units, likewise **Z48**, but due to the strong π-conjugation over the entire array.

Two-Dimensional Cyclic Porphyrin Array

Excitonic and Electronic Coupling of CZ*n*. To mimic two-dimensional EET process of natural LH1 and LH2,[6,13] we have constructed the directly-linked cyclic porphyrin arrays **CZ***n* of different wheel sizes (Chart 1).[14] The EET

Figure 5. (a) *I-V* curves measured at room temperature on **Z48** (inset is *I-V* curve under illumination with a red LED). (b) *I-V* curves measured at various temperatures on **T8**. Reproduced with permission from ref 12.
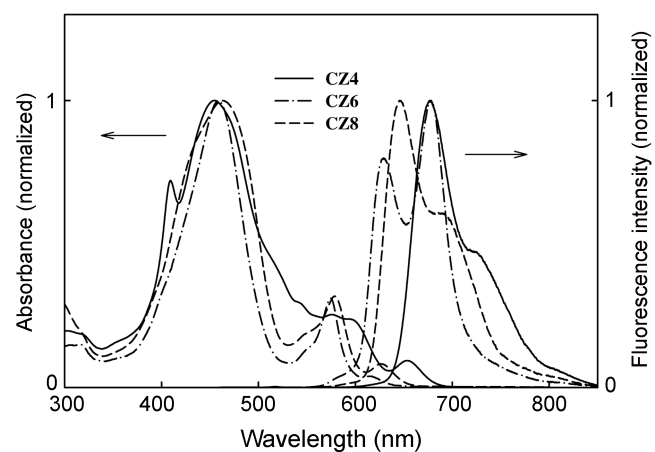

Figure 6. Steady-state absorption (left) and fluorescence (right) spectra of **CZ4**, **CZ6**, and **CZ8**. The fluorescence spectra were obtained with the excitation wavelength 420 nm. Reproduced with permission from ref 14.

process of **CZn** has been examined by femtosecond transient absorption (TA) and transient absorption anisotropy (TAA).

While **Zn** arrays show split Soret ($S_0 \rightarrow S_2$) bands due to the exciton coupling between porphyrin units (Scheme 1),[8b,c] **CZn** exhibit characteristic broad non-split Soret bands that are centered around 460 nm (Figure 6). This observation is explained in terms of symmetric cyclic structure, in which both the B_x and B_y dipole moments are involved in the exciton coupling.[14] On the other hand, the Q absorption ($S_0 \rightarrow S_1$) and fluorescence ($S_1 \rightarrow S_0$) spectra reveal red shifts in going from **CZ6** to **CZ8** and **CZ4**, indicating different electronic/excitonic couplings between porphyrin units (Figure 6). The electronic coupling can be well related to the dihedral angle between the adjacent porphyrin units. The strapped diporphyrin, where the strapping carbon chain controls a dihedral angle between two porphyrin units, shows that the smaller dihedral angle between porphyrin units gives rise to the stronger electronic coupling and concomitantly red shifts in the Q absorption and fluorescence spectra.[15] Consequently, the Q absorption and fluorescence spectra indicate that the electronic coupling strength increases in order of **CZ6** < **CZ8** < **CZ4** in accordance with the dihedral angle estimated from the ^{1}H NMR data and geometry optimization.[14] Because **CZn** have strong excitonic and electronic couplings between porphyrin units, the coherent and/or incoherent EET process can easily be expected. In addition, the relatively long S_1-state lifetimes (~1.8 ns) of **CZn** revealed by the time-correlated single photon counting (TCSPC) measurements are also advantageous in EET process.[14]

EET Process in CZn. To explore the EETs of **CZn**, femtosecond time-resolved transient absorption (TA) and transient absorption anisotropy (TAA) decays were simultaneously measured, where the Q band excitation ($\lambda_{pump} =$

Table 1. Transient absorption decay parameters for CZn depending on pump power[a]

Pump power (mW)	Fitted Decay Times (ps)[b]	
	τ_1	τ_2
CZ4		
2.0	0.073 (14%)	1840 (86%)
1.0	0.073 (9%)	1840 (91%)
0.5	0.073 (8%)	1840 (92%)
CZ6		
2.0	0.56 (17%)	1760 (83%)
1.0	0.56 (13%)	1760 (87%)
0.5	0.56 (11%)	1760 (89%)
CZ8		
2.0	0.66 (44%)	1800 (56%)
1.0	0.70 (35%)	1800 (65%)
0.5	0.68 (19%)	1800 (81%)

[a]The pump and probe wavelengths are 583 and 460 nm, respectively. [b]Using the relation $-\Delta OD(t) = A_1 \exp(-t/\tau_1) + A_2 \exp(-t/\tau_2)$, where $\Delta OD(t)$ is the transient absorption intensity, A the amplitude (noted in parentheses as the normalized percentage *i.e.* $[A_i/(A_1 + A_2)] \times 100$), and τ the fitted decay time. The solvent used was consistently THF.
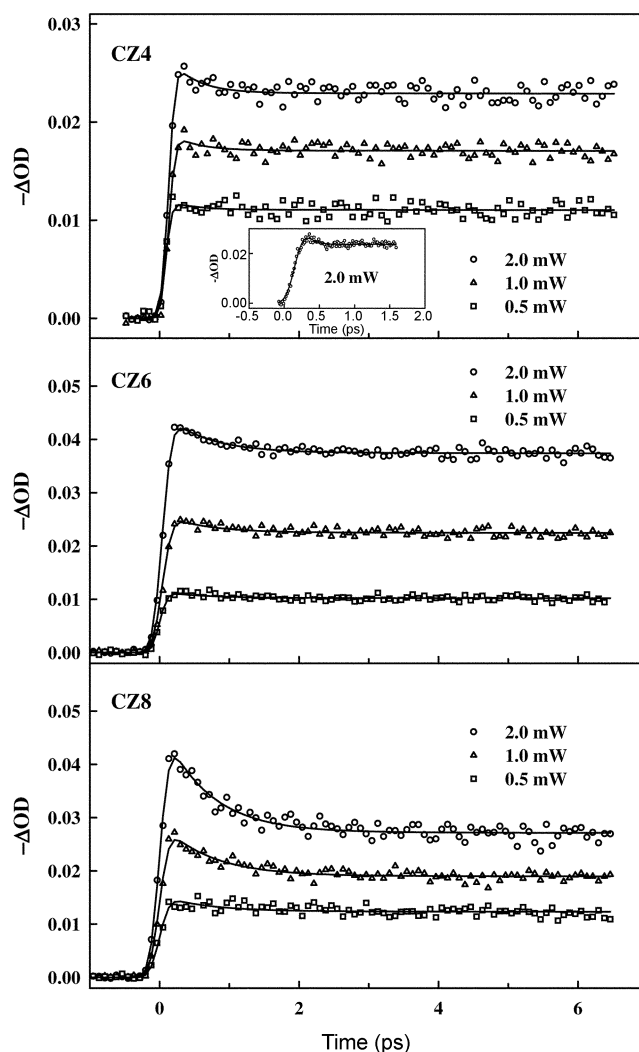

Figure 7. Transient absorption decay profiles of **CZ4**, **CZ6**, and **CZ8** that include pump power dependences, where the pump and probe wavelengths are 583 and 460 nm, *i.e.*, Q band pump and bleaching recovery probe. The decays were measured with magic angle polarization between pump and probe beams in THF. Reproduced with permission from ref 14.

583 nm) was employed to avoid an involvement of S_2-S_1 relaxation in the porphyrin (Figures 7 and 8). As displayed, **CZn** reveal pump power dependent TA-decays along with TAA-rises in the time scale of hundreds of femtoseconds. The TA-decays are deconvoluted with two decay components (τ_1 and τ_2), where the slow τ_2 components are fixed as the S_1-state lifetimes found in the TCSPC measurements (Table 1). The TAA-rises are also deconvoluted with one rise component, of which the fitted parameters are inserted in Figure 8.

The TA-decay depends on the pump power as well as the size of **CZn** (Figure 7 and Table 1). As the pump power is increased, the relative contribution of fast τ_1 component is enhanced as compared with the long-lived one. In addition, the τ_1 value systematically increases from 73 fs to 560 fs and 680 fs in going from **CZ4** to **CZ6** and **CZ8**, *i.e.*, as the size of **CZn** increases. The pump-power dependence on the TA-
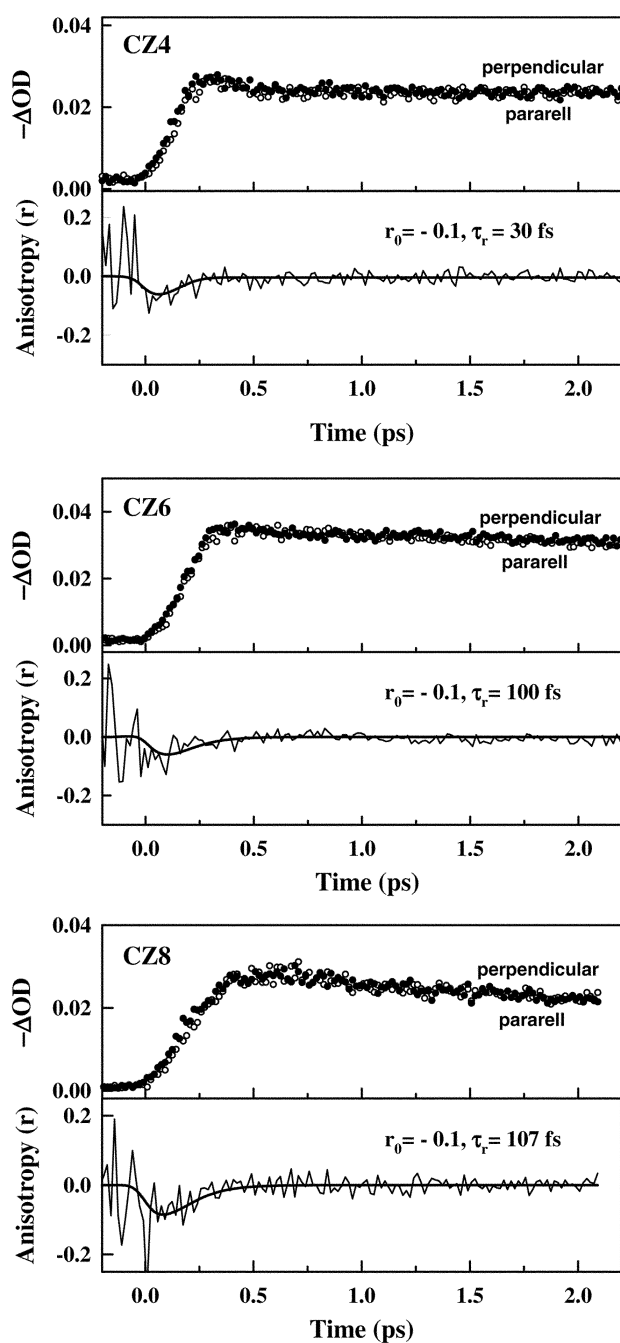
Figure 8. Transient absorption anisotropy decay profiles of **CZ4**, **CZ6**, and **CZ8**, where the polarized transient absorption decays for parallel and perpendicular orientations between pump and probe beams are included. Insets show the deconvolution fitted decay parameters with a train of 150-fs pump pulse. The pump and probe wavelengths are 583 and 460 nm, which are *Q* band pump and bleaching recovery probe. The solvent used was THF. Reproduced with permission from ref 14.

decay is indicative of S_1-S_1 exciton-exciton annihilation, because intense excitation or high density of photons generates two or more excitons in one cyclic array, and then the recombination between excitons creates fast deactivation channel.[16,17] Figure 7 and Table 1 indicate that the exciton-exciton annihilation is due to the migration limited exciton-exciton recombination process along **CZ*n***, because this

process becomes slower as the size of traveling ring increases. It is interesting to note that the exciton migration time of 680 fs in **CZ8** is even faster than ~1 ps[16] in natural LH2.

The TAA measurement was employed to characterize the EET rate, because the EET process even between the same molecular units aligned in different direction creates a depolarization channel. Figure 8 shows the TAA-rises arising from the fast energy migration processes of **CZ*n***. The TAA rise-time systematically increases from 30 fs to 100 fs and 107 fs in going from **CZ4** to **CZ6** and **CZ8**, indicating the dependence on the traveling ring size.
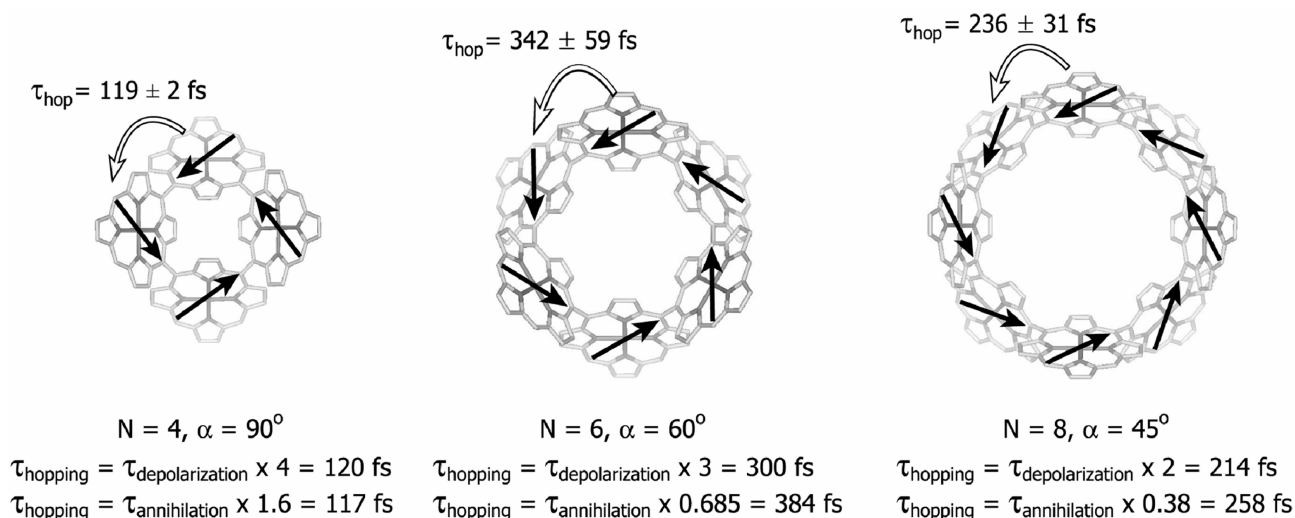
In multi-chromophoric system, neither exciton-exciton annihilation nor anisotropy depolarization time does directly represent the EET time, because they do not occur in single donor-acceptor pair. The EET time between the constituent pigments can be theoretically evaluated by modeling the hopping process and simultaneous observation of these two observables.[16,17] The exciton-exciton annihilation and anisotropy depolarization have been well developed for the natural light-harvesting cyclic LH1 and LH2 systems by G. R. Fleming *et al.*[16] When Förster-type incoherent EET model was employed by assuming a migration-limited character of exciton-exciton annihilation, and a random walk formalism of the anisotropy decay, the analytical depolarization and exciton-exciton annihilation times were connected with the excitation energy transfer or hopping (EET or EEH) time by eqs 4 and 5,

$$\tau_{depolarization} = \frac{\tau_{hopping}}{4(1 - \cos^2(2\pi/N))} = \frac{\tau_{hopping}}{4(1 - \cos^2\alpha)} \quad (4)$$

$$\tau_{annihilation} = \frac{N^2 - 1}{24} \tau_{hopping} \quad (5)$$

where N is the number of hopping sites, α the angle between the adjacent transition dipoles, $\tau_{annihilation}$ the slowest exciton-exciton annihilation time, and $\tau_{hopping}$ the inverse of the nearest neighbor EET rate.[16,17] Eq. 4 is understood by considering that the depolarization is complete when the transition dipole migrates through 90° and by considering how many hops are required for this rotation to be accomplished. On the other hand, eq. 5 assumes that the exciton-exciton annihilation reflects the migration limited exciton-exciton recombination process along the cyclic array and how many hops are required for this recombination to be accomplished.

Now, we model the EET process within **CZ*n***, and simultaneously use the two different observables, exciton-exciton annihilation and anisotropy decay times, to estimate the EET times. Concerning the number of hopping sites, it is conceived as N = 4, N = 6, and N = 8 for **CZ4**, **CZ6** and **CZ8**, respectively. Although the exciton coherence via two porphyrin units rather than one porphyrin unit is rationalized in **CZ*n***, in view of cyclic geometry and exciton coherence length of 4.5 porphyrin units of **Z*n***, the number of hopping sites would be N = 4, N = 6, and N = 8, resulting from the

$\tau_{hop} = 119 \pm 2$ fs

$\tau_{hop} = 342 \pm 59$ fs

$\tau_{hop} = 236 \pm 31$ fs

N = 4, $\alpha = 90°$

$\tau_{hopping} = \tau_{depolarization}$ x 4 = 120 fs

$\tau_{hopping} = \tau_{annihilation}$ x 1.6 = 117 fs

N = 6, $\alpha = 60°$

$\tau_{hopping} = \tau_{depolarization}$ x 3 = 300 fs

$\tau_{hopping} = \tau_{annihilation}$ x 0.685 = 384 fs

N = 8, $\alpha = 45°$

$\tau_{hopping} = \tau_{depolarization}$ x 2 = 214 fs

$\tau_{hopping} = \tau_{annihilation}$ x 0.38 = 258 fs

Scheme 2. Excitation energy hopping rate in **CZ*n***. Reproduced with permission from ref 14.

bidirectional coupling between the neighboring porphyrins in two-dimensional space of **CZ*n***.[14] In order to describe the random walk of the anisotropy decay, the orientations of the molecular transition dipole moments should be considered. As shown in Scheme 2, the transition dipoles that are attributable to the change in anisotropy are arranged in two-dimensional xy-plane, where the anisotropy decay profile reflects the EET process among the transition dipoles. This modeling indicates that the EET process of **CZ*n*** can be well described by eqs. 4 and 5, which are applicable to a well-defined cyclic molecular array. Introducing N = 4 and $\alpha = 90°$ to eqs 4 and 5, the relations $\tau_{hopping} = 4 \times \tau_{depolarization}$ and $\tau_{hopping} = 1.6 \times \tau_{annihilation}$ are obtained for **CZ4**. Similarly, introducing N = 6 and $\alpha = 60°$, the relations $\tau_{hopping} = 3 \times \tau_{depolarization}$ and $\tau_{hopping} = 0.685 \times \tau_{annihilation}$ are obtained for **CZ6**. Finally, introducing N = 8 and $\alpha = 45°$, the relations $\tau_{hopping} = 2 \times \tau_{depolarization}$ and $\tau_{hopping} = 0.38 \times \tau_{annihilation}$ are obtained for **CZ8**. Consequently, the EET time constants are calculated to be 120, 300, and 214 fs in **CZ4**, **CZ6**, and **CZ8**, respectively, using the anisotropy rise times of $\tau_r = 30$, 100, and 107 fs, given in Figure 8. In a different approach, the EET time constants are estimated to be 117, 384, 258 fs using the exciton-exciton annihilation times of $\tau_1 = 73$, 560, and 680 fs, given in Table 1. It is noteworthy that the two different experimental observables, exciton-exciton annihilation and anisotropy depolarization, result in the same EET times within error ranges, which are 119 ± 2 fs in **CZ4**, 342 ± 59 fs in **CZ6**, and 236 ± 31 fs in **CZ8** (Scheme 2). This coincidence implies that the EET process are well described by Förster-type incoherent energy hopping model, because of their well-defined dipole orientations. Finally, the observed EET times (119 ± 2 fs in **CZ4**, 342 ± 59 fs in **CZ6**, and 236 ± 31 fs in **CZ8**) can be well associated with the red-shifts in the Q absorption and fluorescence spectra, demonstrating that the increased electronic interaction accelerates the EET process between porphyrin units. We attribute this trend primarily to the decreased dihedral angle between the neighboring porphyrins in order of **CZ6** > **CZ8** > **CZ4**.

Finally, it is interesting to note that the EET times, *i.e.*, 119 ± 2 fs in **CZ4** and 236 ± 31 fs in **CZ8** are faster than ~270 fs[17a] in natural LH2, because of the proximity and stronger electronic couplings in **CZ*n***. Consequently, the EET dynamics of **CZ*n***, as investigated by femtosecond TA and TAA measurements, have proposed cyclic molecular systems as suitable artificial photosynthetic antenna or optoelectronic medium in terms of a lack of energy sink and highly efficient EETs.

Three-Dimensional Porphyrin Box

Supramolecular Self-Assembly. As shown in Chart 1, three-dimensional zinc(II) porphyrin boxes **B*n*** were prepared by self-assembly of *meso-meso*-pyridine-appended zinc(II) diporphyrins **D*n***, where the size of **B*n*** was controlled by inserting one and two phenyl groups between the porphyrin and pyridyl substituents, *i.e.*, **D*n*** = **Py(Ph)$_{n-1}$Z2**.[18c] The self-assembly is driven by intermolecular coordination between zinc(II) central metal ion of **D*n*** and peripheral pyridine-appended group of neighboring **D*n***. Because the inter-molecular coordination among **D*n*** molecules competes with solvent coordination as an axial ligand of zinc(II) porphyrin, the box formation inevitably depends upon the solvent coordination.[18] Specifically, CH_2Cl_2 does not have a capability to coordinate with zinc(II) pophyrin due to its absence of non-paired electrons, while pyridine can coordinate with zinc(II) porphyrin due to its non-paired electrons. As a consequence, the box formation only occurs in CH_2Cl_2, in which the intermolecular coordination predominantly occurs over the solvent coordination. In the present study, **D*n*** molecules dissolved in strongly coordinating pyridine have been taken as references of five coordinated free *meso-meso* linked zinc(II) diporphyrins and those dissolved in non-coordinating CH_2Cl_2 have been used for the measurements of **B*n***.

Exciton Coupling of B*n*. Figure 9 shows the absorption and fluorescence spectra of (a) **D*n*** in pyridine and (b) **B*n*** in
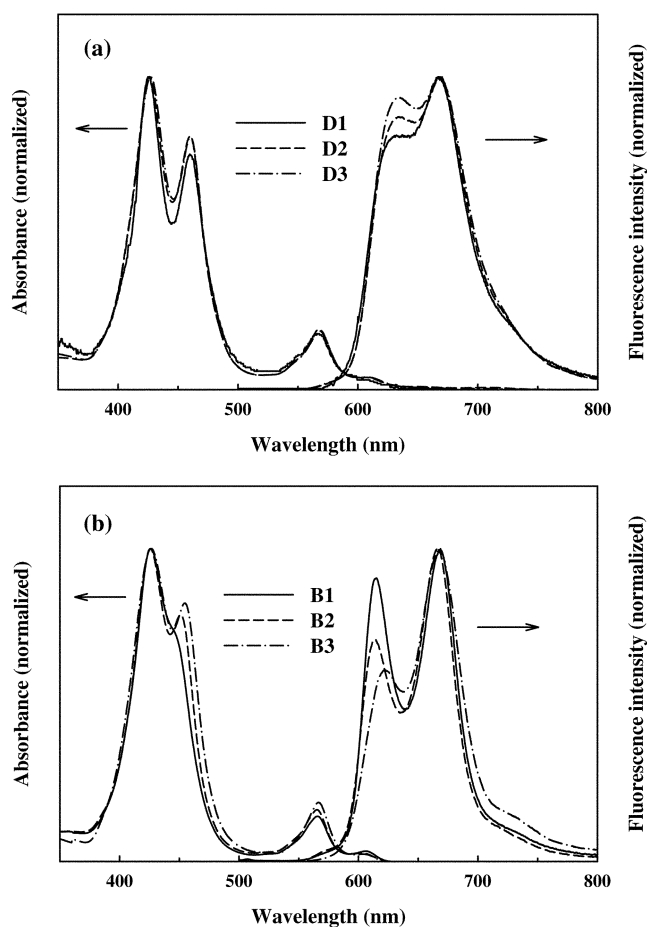
Figure 9. Steady-state absorption (left) and fluorescence (right) spectra of (a) **D***n* in pyridine and (b) **B***n* in CH₂Cl₂. The fluorescence spectra were obtained with the excitation wavelength 430 nm, and the excitation wavelength dependence on the fluorescence spectra was negligible. Reproduced with permission from ref 18c.

Figure 10. Transient absorption decay profiles of **B***n* that include pump power dependence. The transient absorption decay profiles of **D***n* are inserted in the rights of the Figures. In the experiments, the pump and probe wavelengths were 570 and 490 nm, which are the *Q* band pump and induced absorption probe. Reproduced with permission from ref 18c.

CH₂Cl₂. As displayed, **B***n* show much smaller split Soret bands than those of **D***n*, for which the extent of split also exhibits systematic change depending on the size of box. While the high energy Soret band remains at the same position, the low energy Soret band shifts to blue in order of **B3** < **B2** < **B1**. In fluorescence, **B***n* show narrower bands than those of **D***n*.

The fluorescence spectora of **B***n* are explained in terms of small electronic interaction between the two porphyrin units in *meso-meso* linked zinc(II) diporphyrin component, which is brought about as *rigidification of its perpendicular conformation* upon the box formation.[18] On the other hand, the absorption spectra of **B***n* are qualitatively explained by the exciton coupling theory.[10] The Soret band splitting in the *meso-meso* linked zinc(II) diporphyrin is explained by simple excitonic dipole coupling between zinc(II) porphyrin monomers (Scheme 1).[8b,c] In the case of **B***n*, however, much complicated Soret band splits occur because of various dipole-dipole excitonic interactions among eight mutually perpendicular porphyrin units.[18b,c] Among sixteen possible exciton coupling states, only two states are transition-
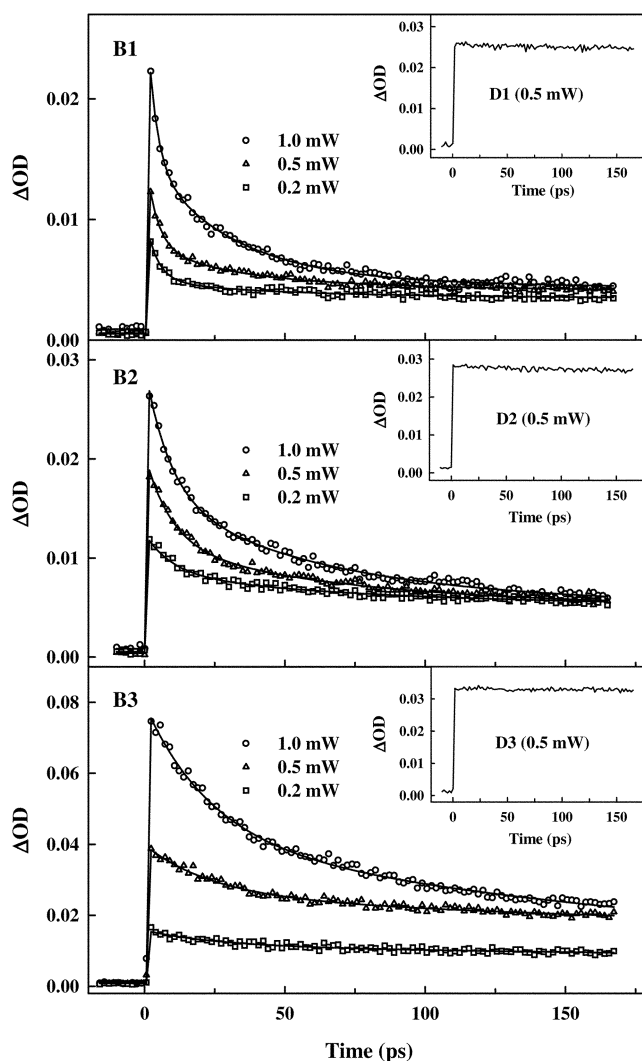
allowed for **B***n*. The low energy Soret state indicates excitonic dipole-dipole interaction among eight parallel transition dipole moments along the z-axis of Scheme 1, whereas the high energy Soret state implies excitonic dipole-dipole interaction among four parallel transition dipole moments along the x- or y-axis of Scheme 1 (Scheme 1, right).[18b,c] Using the reported transition dipole strength (9.5 ± 0.5 D)[19] of the Soret band of the pyridyl-substituted zinc(II) porphyrin monomer (5-(4-pyridyl)-triphenylporphyrin), the porphyrin center-to-center distances ($8 \times 8 \times 10$ Å³), and the dipole orientations, the excitonic Soret band splitting energy ΔE_{Soret} of **B1** was calculated to be ~1112 cm⁻¹, in good agreement with the experimental splitting value of 1129 cm⁻¹.[18b,c]

The blue shift in the low-energy Soret band of **B1** is due to the H-type dipole coupling among four parallel transition dipoles along the z-axis of Scheme 1. The H-type dipole coupling, thus, is expected to decrease in going from **B1** to
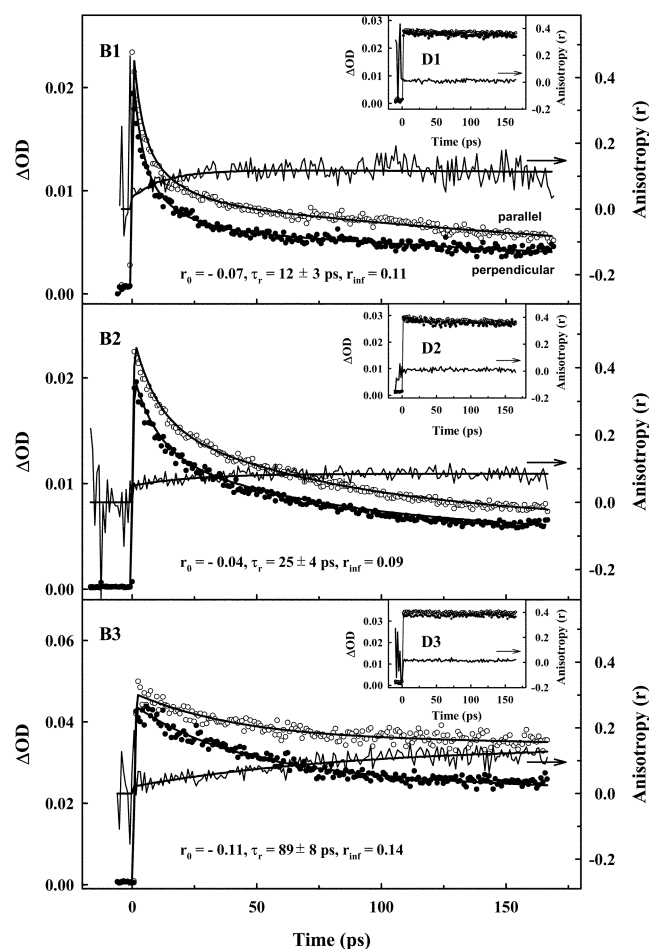
Figure 11. Transient absorption anisotropy decay profiles of **B***n*; the transient absorption decays for parallel and perpendicular orientations between pump and probe polarizations are included, and the fitted decay parameters are inserted. The transient absorption anisotropy decay profiles of **D***n* are presented in the rights of the Figures. The pump and probe wavelengths were 570 and 490 nm, respectively. Reproduced with permission from ref 18c.

B2 and **B3**, resulting in the small blue shift of the low-energy Soret band. The excitonic Soret band splitting energies ΔE_{Soret} of **B2** and **B3** were calculated by the similar procedures to that of **B1**, in which the different geometrical parameters ($8 \times 14 \times 14$ Å^3 for **B2** and $8 \times 18 \times 18$ Å^3 for **B3**) gave rise to the ΔE_{Soret} values of ~1635 and ~1741 cm^{-1} for **B2** and **B3**, respectively, which were larger than ~1112 cm^{-1} of **B1**.[18c] Consequently, the exciton coupling strength can be tuned by changing the size of **B***n*, because the interchromophoric distance concomitantly changes.

EET Process in B*n*. The EETs of **B***n* were comparatively investigated by femtosecond TA and TAA measurements, where the *Q* band excitation, *i.e.*, λ_{pump} = 570 nm was employed to avoid an involvement of S$_2$-S$_1$ relaxation (Figures 10 and 11). The TA and TAA decays of **D***n* were also measured as references. As displayed, **D***n* reveal slow TA decays, in agreement with the S$_1$-state lifetimes (~1.6-1.8 ns) revealed by the TCSPC measurements, and concomitantly do not show any anisotropy decay profiles in the time region

**Table 2**. Transient absorption decay parameters for B*n* depending on pump power[a]

Pump power (mW)	Fitted Decay Times (ps)[b]		
	τ_1	τ_2	τ_3
B1			
1.0	3 (44%)	30 (40%)	1610 (16%)
0.5	4 (46%)	30 (24%)	1610 (30%)
0.2	4 (48%)	30 (14%)	1610 (38%)
B2			
1.0	9 (42%)	57 (39%)	1670 (19%)
0.5	9 (42%)	60 (29%)	1670 (29%)
0.2	10 (31%)	59 (22%)	1670 (47%)
B3			
1.0	24 (48%)	230 (47%)	1750 (5%)
0.5	25 (37%)	228 (19%)	1750 (44%)
0.2	26 (30%)	228 (16%)	1750 (54%)

[a]The pump and probe wavelengths are 570 and 490 nm, respectively. [b]Using the relation $\Delta OD(t) = A_1 \exp(-t/\tau_1) + A_2 \exp(-t/\tau_2) + A_3 \exp(-t/\tau_3)$, where $\Delta OD(t)$ is the transient absorption intensity, *A* the amplitude (noted in parentheses as the normalized percentage *i.e.* $[A_i/(A_1 + A_2 + A_3)] \times 100$), and τ the fitted decay time. The solvent used was CH$_2$Cl$_2$.

of tens of picosecond (Insets of Figures 10 and 11). On the other hand, **B***n* show relatively fast TA decays along with anisotropy rises, indicating fast depolarization channels due to the EET process. The exponential fittings for the TA decays of **B***n* were performed with three decay components (τ_1, τ_2, and τ_3), where the slowest decay ones were fixed as the S$_1$-state lifetimes found in the TCSPC measurements (Table 2). The TA decays of **B***n* are dependent upon both the pump-power and the molecule. When the pump power was increased, the relative contributions of fast τ_1 and τ_2 components were enhanced as compared to that of τ_3 one. In addition, both τ_1 and τ_2 values systematically increases in order of **B1** < **B2** < **B3** (Table 2). The pump-power dependence on the decay is indicative of S$_1$-S$_1$ exciton-exciton annihilation, similarly to **CZ***n*. In addition, Figure 10 indicates that the exciton-exciton annihilation is due to the exciton-exciton recombination between *meso-meso* linked zinc(II) diporphyrins rather than zinc(II) porphyrin monomers, because this process does not occur in **D***n* and it becomes slower, as the distance between *meso-meso* linked zinc(II) diporphyrins increases.

The TAA decays of **B***n* were fitted with one rise component, *i.e.*, 12 ps in **B1**, 25 ps in **B2**, and 89 ps in **B3** (Figure 11). Increasing TAA rise-time constant in order of **B1** < **B2** < **B3** indicates that instead of energy hopping within a *meso-meso* linked zinc(II) diporphyrin, energy transfer between neighboring *meso-meso* linked zinc(II) diporphyrins is responsible for this anisotropic rise. Here we note that the TAA of **B***n* shows a single exponential rise component τ_r, even though the TA of **B***n* reveals the two exciton-exciton annihilation components τ_1 and τ_2. The discrepancy between the exciton-exciton annihilation and the anisotropy depolarization, however, has been often found in other multi-chromophoric systems such as natural LH1 and LH2.[16,17]
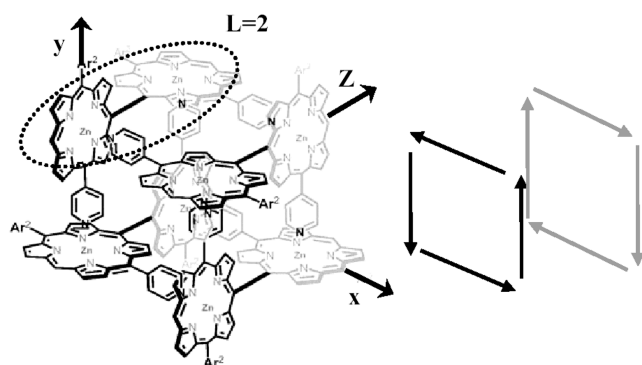
Scheme 3. Energy hopping model of **B***n*. Reproduced with permission from ref 18c.

The EET times of **B***n* were estimated by modeling the energy migration and simultaneous use of two different observables *e.g.* exciton-exciton annihilation and anisotropy depolarization times, which is similar to **CZ***n*. **B***n* are regarded as a cyclic multi-porphyrin array that consists of four mutually perpendicular *meso-meso* linked zinc(II) diporphyrins. They have eight mutually perpendicular porphyrin units, however, the number of hopping sites is N = 4, because the hopping sites are four *meso-meso* linked zinc(II) diporphyrins that have the exciton coherence lengths of L = 2 (Scheme 3). Although the exciton coherence length of **Z***n* is L = 4.5,[8b,c] **B***n* has the exciton coherence length of L = 2, because of the noncovalent linkages. In order to describe the random walk of the anisotropy, the orientation of the molecular transition dipoles was considered. As shown in Scheme 3, the transition dipoles that are attributable to the change of anisotropy are arranged in a rectangular cycle on xy-plane; the energy hopping process among the transition dipoles along z-axis does not change the anisotropy (Scheme 1, right). Consequently, the anisotropy decay profile of **B***n* reflects the EET process in forward (black) or backward (gray) rectangular cycle that consists of mutually perpendicular four transition dipole moments. This modeling indicates that the EET process of **B***n* can also be well described by eqs 4 and 5. Introducing N = 4 and $\alpha = 90°$, the relations $\tau_{hopping} = 4 \times \tau_{depolarization}$ and $\tau_{hopping} = 1.6 \times \tau_{annihilation}$ are obtained for **B***n*. As consequence, the energy hopping times are calculated to be 48, 100, and 356 ps in **B1**, **B2**, and **B3** using the anisotropy rise-times (τ_r = 12, 25, and 89 ps), given in Figure 11. In a different approach, the energy hopping times are estimated to be 48, 96, 365 ps using the slowest exciton-exciton annihilation components (τ_2 = 30, 60, and 228 ps), listed in Table 2, where the slowest annihilation component[16,17] describes the migration limited exciton-exciton recombination process along **B***n*. Consequently, the two different observables resulted in the consistent EET times within very small error ranges (48 ps in **B1**, 98 ± 3 ps in **B2**, and 361 ± 6 ps in **B3**). This implies that the excitation energy migration process within **B***n* is excellently described by the Förster-type incoherent energy hopping model, because of their well-defined and rigid perpendicular orientations. In addition, the EET rate is well controlled by adjusting the exciton coupling strength between the constituent pigments.

Conclusions

The time-resolved optical measurements were conducted to characterize the rate and yield of the EET process occurring in various forms of porphyrin arrays (linear, cycle, and box). The obtained results demonstrate that the competition in EET process can be modulated by the choice of the array and also, by inference, the exciton coupling in the array. This provides an avenue for achieving different properties and functions of optoelectronic materials based on porphyrin arrays. The fundamental information about the excited-state dynamics and decay pathways was also essential for the proper interpretation of the EET processes in the more complex arrays, such as two- and three-dimensional porphyrin arrays. The novel porphyrin arrays envisaged will make use of tuned photophysical properties to develop specific molecular devices.

References

1. McDermott, G. M.; Prince, S. M.; Freer, A. A.; Hawthonthwaite-Lawless, A. M.; Papiz, M. Z.; Cogdell. R. J.; Isaacs, M. W. *Nature* **1995**, *374*, 517.
2. Pullerits, T.; Sundström, V. *Acc. Chem. Res.* **1996**, *29*, 381.
3. Holten, D.; Bocian, D. F.; Lindsey, J. S. *Acc. Chem. Res.* **2002**, *35*, 57 and references are therein.
4. Kim, D.; Osuka, A. *Acc. Chem. Res.* **2004**, *37*, 735 and references are therein.
5. (a) Kim, D.; Osuka, A. *J. Phys. Chem. A* **2003**, *107*, 8791 and references are therein. (b) Song, N. W.; Cho, H. S.; Yoon, M.-C.; Aratani, N.; Osuka, A.; Kim, D. *Bull. Korean Chem. Soc.* **2002**, *23*, 271.
6. Cho, H. S.; Rhee, H.; Song, J. K.; Min, C.-K.; Takase, M.; Aratani, N.; Cho, S.; Osuka, A.; Joo, T.; Kim, D. *J. Am. Chem. Soc.* **2003**, *125*, 5849.
7. (a) Hayashi, T.; Ogoshi, H. *Chem. Soc. Rev.* **1997**, *26*, 355. (b) Imamura, T.; Fukushima, K. *Coord. Chem. Rev.* **2000**, *198*, 133. (c) Wojaczynski, J.; Latos-Grazynski, L. *Coord. Chem. Rev.* **2000**, *204*, 113. (d) Chernook, A. V.; Rempel, U.; van Borczyskowski, C.; Shulga, A. M.; Zenkevich, E. I. *Chem. Phys. Lett.* **1996**, *254*, 229. (e) Flamigni, L.; Johnson, M. R. *New. J. Chem.* **2001**, *25*, 1368. (f) Hartnell, R. D.; Arnold, D. P. *Organometallics* **2004**, *23*, 391.
8. (a) Aratani, N.; Osuka, A.; Kim, D.; Kim, Y. H.; Jeong, D. H. *Angew. Chem. Int. Ed.* **2000**, *39*, 1458. (b) Cho, H. S.; Song, N. W.; Kim, Y. H.; Jeoung, S. C.; Hahn, S.; Kim, D.; Kim, S. K.; Yoshida, N.; Osuka, A. *J. Phys. Chem. A* **2000**, *104*, 3287. (c)

Kim, Y. H.; Jeong, D. H.; Kim, D.; Jeoung, S. C.; Cho, H. S.; Kim, S. K.; Aratani, N.; Osuka, A. *J. Am. Chem. Soc*. **2001**, *123*, 76. (d) Kim, Y. H.; Cho, H. S.; Kim, D.; Kim, S. K.; Yoshida, N.; Osuka, A. *Syn. Metal* **2001**, *117*, 183. (e) Aratani, N.; Osuka, A.; Cho, H. S.; Kim, D. *J. Photochem. Photobiol. C: Photochem. Rev.* **2002**, *3*, 25. (f) Min, C.-K.; Joo, T.; Yoon, M.-C.; Kim, C. M.; Hwang, Y. N.; Kim, D.; Aratani, N.; Yoshida, N.; Osuka, A. *J. Chem. Phys.* **2001**, *114*, 6750. (g) Cho, H. S.; Jeong, D. H.; Yoon, M.-C.; Kim, Y.-R.; Kim, D.; Jeoung, S. C.; Kim, S. K.; Aratani, N.; Shinmori, H.; Osuka, A. *J. Phys. Chem. A* **2001**, *105*, 4200. (h) Jeong, D. H.; Yoon, M.-C.; Jang, S. M.; Kim, D.; Cho, D. W.; Yoshida, N.; Aratani, N.; Osuka, A. *J. Phys. Chem. A* **2002**, *106*, 2359. (i) Aratani, N.; Cho, H. S.; Ahn, T. K.; Cho, S.; Kim, D.; Sumi, H.; Osuka, A. *J. Am. Chem. Soc.* **2003**, *125*, 9668. (j) Yoon, M.-C.; Song, J. K.; Cho, S.; Kim, D. *Bull. Korean Chem. Soc.* **2003**, *24*, 1075. (k) Song, N. W.; Cho, H. S.; Yoon, M.-C.; Jeoung, S. C.; Yoshida, N.; Osuka, A.; Kim, D. *Bull. Korean Chem. Soc.* **2002**, *75*, 1023.

9. (a) Tsuda, A.; Osuka, A. *Science* **2001**, *293*, 79. (b) Cho, H. S.; Jeong, D. H.; Cho, S.; Kim, D.; Matsuzaki, Y.; Tanaka, K.; Tsuda, A.; Osuka, A. *J. Am. Chem. Soc.* **2002**, *124*, 14642. (c) Jeong, D. H.; Jang, S. M.; Hwang, I.-W.; Kim, D.; Matsuzaki, Y.; Tanaka, K.; Tsuda, A.; Nakamura, T.; Osuka, A. *J. Chem. Phys.* **2003**, *119*, 5237.

10. (a) Kasha, M. *Radiation Res.* **1963**, *20*, 55. (b) Kasha, M.; Rawls, H. R.; El-Bayoumi, M. A. *Pure Appl. Chem.* **1965**, *11*, 371. (c) Scholes, G. D.; Ghiggino, K. P. *J. Phys. Chem.* **1994**, *98*, 4580.

11. (a) Kakitani, T.; Kimura, A. *J. Phys. Chem. A* **2002**, *106*, 2173. (b) Kimura, A.; Kakitani, T.; Yamato, T. *J. Phys. Chem. B* **2000**, *104*, 9276. (c) Ha, J.-H.; Cho, H. S.; Song, J. K.; Kim, D.; Aratani, N.; Osuka, A. *Chem. Phys. Chem.* **2004**, *5*, 57.

12. Yoon, D. H.; Lee, S. B.; Yoo, K.-H.; Kim, J.; Lim, J. K.; Aratani, N.; Tsuda, A.; Osuka, A.; Kim, D. *J. Am. Chem. Soc.* **2003**, *125*, 11062.

13. Peng, X.; Aratani, N.; Takagi, A.; Matsumoto, T.; Kawai, T.; Hwang, I.-W.; Ahn, T. K.; Kim, D.; Osuka, A. *J. Am. Chem. Soc.* **2004**, *126*, 4468.

14. Nakamura, Y.; Hwang, I.-W.; Aratani, N.; Ahn, T. K.; Ko, D. M.; Takagi, A.; Kawai, T.; Matsumoto, T.; Kim, D.; Osuka, A. *J. Am. Chem. Soc.* **2005**, *127*, 236.

15. (a) Yoshida, N.; Jeong, D. H.; Cho, H. S.; Kim, D.; Matsuzaki, Y.; Tanaka, K.; Osuka, A. *Chem. Eur. J.* **2003**, *9*, 58. (b) Jeong, D. H.; Jang, S. M.; Hwang, I.-W.; Kim, D.; Yoshida, N.; Osuka, A. *J. Phys. Chem. A* **2002**, *106*, 11054. (c) Cho, H. S.; Song, J. K.; Ha, J.-H.; Cho, S.; Kim, D.; Yoshida, N.; Osuka, A. *J. Phys. Chem. A* **2003**, *107*, 1897. (d) Shinmori, H.; Ahn, T. K.; Cho, H. S.; Kim, D.; Yoshida, N.; Osuka, A. *Angew. Chem. Int. Ed.* **2003**, *42*, 2754.

16. Bradforth, S. E.; Jimenez, R.; van Mourik, F.; van Grondelle, R.; Fleming, G. R. *J. Phys. Chem.* **1995**, *99*, 16179.

17. (a) Trinkunas, G.; Herek, J. L.; Polívka, T.; Sundström, V.; Pullerits, T. *Phys. Rev. Lett.* **2001**, *86*, 4167. (b) Trinkunas, G. *J. Luminescence* **2003**, *102*, 532. (c) Brüggemann, B.; May, V. *J. Chem. Phys.* **2004**, *120*, 2325. (d) Müller, M. G.; Hucke, M.; Reus, M.; Holzwarth, A. R. *J. Phys. Chem.* **1996**, *100*, 9537. (e) Brüggemann, B.; Herek, J. L.; Sundström, V.; Pullerits, T.; May, V. *J. Phys. Chem. B* **2001**, *105*, 11391.

18. (a) Tsuda, A.; Nakamura, T.; Sakamoto, S.; Yamaguchi, K.; Osuka, A. *Angew. Chem. Int. Ed.* **2002**, *41*, 2817. (b) Hwang, I.-W.; Cho, H. S.; Jeong, D. H.; Kim, D.; Tsuda, A.; Nakamura, T.; Osuka, A. *J. Phys. Chem. B* **2003**, *107*, 9977. (c) Hwang, I.-W.; Kamada, T.; Ahn, T. K.; Ko, D. M.; Nakamura, T.; Tsuda, A.; Osuka, A.; Kim, D. *J. Am. Chem. Soc.* **2004**, *126*, 16187.

19. Yatskou, M. M.; Koehorst, R. B. M.; Donker, H.; Schaafsma, T. J. *J. Phys. Chem. A* **2001**, *105*, 11425.